

IRON GRADIENTS IN COOLING FLOW GALAXIES AND GROUPS

DAVID A. BUOTE¹

UCO/Lick Observatory, University of California at Santa Cruz, Santa Cruz, CA 95064; buote@ucolick.org

Accepted for Publication in The Astrophysical Journal

ABSTRACT

Previous studies of the Fe abundances in the hot gas of galaxies and groups have reported conflicting results with most studies finding very sub-solar Fe abundances that disagree with standard theory. To investigate the possible role of Fe abundance gradients on these measurements we present deprojection analysis of the *ROSAT* PSPC data of 10 of the brightest cooling flow galaxies and groups. The PSPC allows for spatially resolved spectral analysis on a half-arcminute scale, and interesting constraints on both the temperatures and Fe abundances are possible because the ~ 1 keV temperatures of these systems are well matched to the bandpass of the PSPC. In 9 out of 10 systems we find clear evidence that the Fe abundance decreases with increasing radius: $Z_{\text{Fe}} \approx 1Z_{\odot} - (\text{several})Z_{\odot}$ within the central radial bin ($r \lesssim 10$ kpc) which decreases to $Z_{\text{Fe}} \sim 0.5Z_{\odot}$ at the largest radii examined ($r \sim 50$ -100 kpc). The Fe abundances (and temperatures) are consistent with the average values for these systems that we obtained in our previous analyses of the *ASCA* data using multitemperature models which confirms that previous inferences of very sub-solar Fe abundances from *ASCA* arise from the incorrect assumption of isothermal gas and not the presence of Fe abundance gradients. We discuss why this “Fe Bias” affects much more seriously the measurements of Z_{Fe} from *ASCA* data than from *ROSAT* data. We show that the Fe abundance profiles for these galaxies and groups are consistent with a gas-dynamical model where the gas is enriched by stellar ejecta and supernovae in the “solar supernova proportion”, the stars formed with a Galactic IMF, and the gas is diluted by mixing with primordial gas at large radii.

Subject headings: cooling flows – intergalactic medium – X-rays: galaxies

1. INTRODUCTION

One important aspect of the problem of galaxy formation is to understand the connection between the history of star formation and the metal enrichment history of the extended hot gaseous component (e.g., Cavaliere, Giacconi, & Menci 2000). Recent studies have argued that most of the metals produced by star-forming galaxies at high redshifts exist in the hot gaseous halos of galaxies and proto-clusters (e.g., Pettini 1999, 2000). By assuming that the hot gaseous components of nearby rich clusters are a fair representation of the local universe as a whole, Renzini (1997, 2000) has argued that the cluster Fe abundances indicate a prompt initial enrichment of the early universe.

Hence, X-ray observations may be vital for obtaining a complete picture of the history of star formation of the universe. In massive elliptical galaxies the metals injected by previous generations of stars do not escape the gravitational field, and thus the hot gas in these systems records the star formation history via the heating and enrichment of the hot gas by supernovae (e.g., Ciotti et al 1991; David, Forman, & Jones 1991; Loewenstein & Mathews 1991). These systems typically fall into the class of cooling flows (e.g., Fabian 1994).

Unfortunately, reliable constraints on the metal enrichment in such systems are lacking because the metal abundances in the hot gas in cooling flow galaxies and groups determined from previous X-ray studies have yielded conflicting results with most authors finding very sub-solar Fe abundances (see Buote 2000a and references therein).

These low Fe abundances are generally less than the stellar values which implies little or no enrichment from Type Ia supernovae and thus an IMF much flatter than that of the Milky Way (e.g., Arimoto et al 1997; Renzini 1997; Wyse 1997). In contrast, in our recent analyses of the *ASCA* data accumulated within $r \sim 3'$ - $5'$ of the brightest ellipticals and groups we find that the Fe abundances are approximately solar and that the previous inferences of very sub-solar Fe abundances using *ASCA* data are the result of a bias arising from assuming the gas to be isothermal in the presence of significant temperature gradients (Buote & Fabian 1998; Buote 1999, 2000a).

To investigate the possible role of Fe abundance gradients on these measurements we have re-examined the *ROSAT* PSPC data of the brightest galaxies and groups. The PSPC allows for spatially resolved spectral analysis on a half-arcminute scale, and interesting constraints on both the temperatures and Fe abundances are possible because the ~ 1 keV temperatures of these systems are well matched to the bandpass of the PSPC. Moreover, analysis of the PSPC data is much less subject to the “Fe Bias” (Buote, 2000a) which plagues analysis of the *ASCA* data (see §5.1).

We selected for re-analysis all of the galaxies and groups possessing published temperature profiles from *ROSAT* (Forman et al 1993; Ponman & Bertram 1993; David et al 1994; Trinchieri et al 1994; Rangarajan et al 1995; Kim & Fabbiano 1995; Irwin & Sarazin 1996; Jones et al 1997; Trinchieri, Fabbiano, & Kim 1997; Mulchaey & Zabludoff 1998) with the exception of the Pegasus I group (Trinchieri et al, 1997) because of the low S/N. All of these

¹Chandra Fellow

systems have rising temperature profiles and multitemperature *ASCA* spectra usually attributed to cooling flows.

All but one of these *ROSAT* studies determined the temperatures and Fe abundances by fitting a single temperature component to the spectrum in an annulus on the sky. However, each annulus on the sky contains the projection of emission from larger radii which can confuse interpretation because of the substantial temperature gradients. Consequently, we have developed our own deprojection code to obtain three-dimensional spectral parameters.

The paper is organized as follows. In §2 we present the observations and discuss the data reduction. The deprojection procedure is described in §3 and the results for the temperature and Fe abundance profiles are given in §4.2; results for the column densities appear in Buote (2000b, hereafter PAPER1; 2000c, hereafter PAPER3). Discussion of the results and our conclusions are presented in §5.

2. *ROSAT* OBSERVATIONS AND DATA REDUCTION

We obtained *ROSAT* PSPC data from the public data archive maintained by the High Energy Astrophysics Science Archive Research Center (HEASARC). The properties of the observations are listed in Table 1. Except where noted below, these data were reduced using the standard FTOOLS (v4.2) software according to the procedures described in the OGIP Memo OGIP/94-010 (“*ROSAT* data analysis using xselect and ftools”), the WWW pages of the *ROSAT* Guest Observer Facility (GOF) (see <http://heasarc.gsfc.nasa.gov/docs/rosat>), and Plucinsky et al (1993).

The events files of each observation were cleaned of afterpulse signals by removing all events following within 0.35 ms of a precursor. To minimize the particle background contribution only events with Master Veto Rate less than 170 ct s^{-1} were selected (Plucinsky et al, 1993). We corrected the Pulse Invariant (PI) bins of each data set for spatial and long-term temporal gain variations using the most up-to-date calibration files. For the FTOOL PCECOR, which corrects for the variation in the linearity of the PSPC response, we used the in-flight calibration data for the correction.

From visual inspection of the light curve of an observation we identified and removed time intervals of significant enhancements in the count rate in order to obtain a flat distribution of count rate versus time. Such short-term enhancements are typically the result of scattered light from the Sun, auroral X-rays, and enhanced charged particle precipitation (Snowden et al, 1994). The raw and filtered exposure times are listed in Table 1.

The particle background spectrum for an observation was obtained by following the instructions in Plucinsky et al (1993). We developed our own software to perform this task because we identified serious errors in the FTOOLS implementation of the Plucinsky et al procedure (i.e., program PCPARPHA). For our data sets the particle background rate is always much less than that of the diffuse background.

For each observation we obtained a background spectrum from source-free regions far away from the center of the field (typically distances of $45'-50'$). By using a local background estimate residual contamination from solar X-rays and any other long-term background enhancements

(Snowden et al, 1994) are fully accounted for in the ensuing spectral analysis. However, the extended emission of the galaxies and groups do contribute at some level to the flux even at these large radii.

To assess the contribution of galaxy and group emission within the background regions we fit the background spectrum with a model after subtracting the particle background. We represent the cosmic X-ray background by a power law and the Galactic emission by two thermal components following Chen et al (1997). To account for emission from the galaxy or group we include another thermal component with variable temperature. Each component is modified by the Galactic hydrogen column listed in Table 1.

This composite model provides a good fit to the background spectrum for each system. In every case the additional thermal component is required with temperatures ranging from 0.3-1.6 keV. In 8 out of 10 cases this additional component contributes significantly only to energies above ~ 0.5 keV which is consistent with emission from the galaxy or group in question. For these systems we subtract this temperature component from the background when performing spectral analysis (see §4.1.4), and the background rates listed in Table 1 reflect this subtraction. The effect of excluding this extra component in the background on the source spectral parameters is only significant for a few systems, and is noticeable only in the outermost one or two radial bins (see §4.3).

For NGC 5044 and 5846 we obtained $T \sim 0.3$ keV for the extra thermal component and found that it contributed very significantly to the emission in both the soft and hard energy channels. In these cases the extra component probably represents a combination of emission from long-term enhancements in the background (Snowden et al, 1994) with any residual emission from the groups. As a result, we did not subtract out the extra thermal component from the background of these systems.

For NGC 4472 we confirm the finding by Forman et al (1993) that a background spectrum taken from regions $\sim 40'-50'$ from the field center tends to over-subtract energies below ~ 0.3 keV probably because of contamination from unresolved point sources. To compensate for this we took the background from regions just inside the inner ring of the PSPC where the PSF is much smaller which allows us to avoid point sources more effectively. We confine the region to the north of the center of NGC 4472 where the galaxy emission is lower (Irwin & Sarazin, 1996).

3. DEPROJECTION METHOD

The method we use to deproject the X-ray data is the well-established technique pioneered by Fabian et al (1981). This method is non-parametric in that no functional form is assumed for the spatial distribution of the X-ray emission or for any of the associated spectral quantities (temperature, abundances etc.). After first assuming a specific geometry one begins by determining the emission in the bounding annulus and then works inwards by subtracting off the contributions from the outer annuli. For the case of spherical symmetry the volume emission density is related to the surface brightness according to the simple geometric formula given by Kriss, Cioffi, & Canizares (1983).

The assumption of hydrostatic equilibrium is usually in-

TABLE 1
ROSAT OBSERVATIONS

Name	z	N_{H} (10^{20} cm^{-2})	Sequence No	Date (Mo/yr)	Exposure (ks)	Source Count Rate (ct s^{-1})	Background ($\text{ct s}^{-1} \text{ arcmin}^{-2}$)
NGC 507	0.01646	5.2	600254n00	8/92	5.7/5.3	1.1E-1	2.8E-4
			600254a01	1/93	15.3/12.6		
NGC 533	0.01810	3.2	600541n00	7/93	13.0/11.8	9.9E-2	2.9E-4
NGC 1399	0.00483	1.3	600043n00	8/91	53.5/18.7	2.5E-1	4.7E-4
NGC 2563	0.01630	4.3	600542n00	10/93	27.1/20.7	2.2E-2	3.2E-4
			600542a01	4/94	22.9/20.6		
NGC 4472	0.00290	1.7	600248n00	12/92	26.0/22.9	2.7E-1	9.2E-4
NGC 4636	0.00365	1.8	600016n00	12/91	13.1/6.3	3.4E-1	1.0E-3
NGC 4649	0.00471	2.2	600017n00	12/91	14.2/9.8	2.5E-1	1.0E-3
NGC 5044	0.00898	5.0	800020n00	7/91	27.7/19.4	5.9E-1	5.2E-4
NGC 5846	0.00610	4.2	600257n00	7/92	8.8/7.0	1.7E-1	7.8E-4
			600257a01	1/93	5.9/3.9		
HCG 62	0.01460	2.7	800098n00	12/91	19.6/13.2	1.5E-1	8.7E-4

NOTE.—Redshifts are taken from NED. Galactic Hydrogen column densities (N_{H}) are taken from Dickey & Lockman (1990) using the HEASARC w3nh tool. The Exposure column lists first the raw exposure time and second the final filtered exposure (see §2). The source count rate is computed within the central $R = 1'$. Both the source and background rates are computed over 0.2-2.2 keV. For systems with multiple observations the source and background rates are computed from the total data.

corporated into this deprojection procedure in order to obtain the mass and mass deposition rate as well as the spectral parameters (Fabian et al 1981; Sarazin 1986; Arnaud 1988). In the interest of generality we do not make this additional assumption. Hence, the principal assumption in our version of the deprojection procedure is that of spherical symmetry which means that our derived spectral parameters should be considered spherically averaged quantities for systems that have significant ellipticity.

A thorough, up-to-date discussion of this deprojection method is given by McLaughlin (1999), and we refer the reader to that paper for the relevant equations. Since McLaughlin is interested in the globular cluster distribution in M87 he formulates the deprojection algorithm in terms of the number of globular clusters, $\mathcal{N}(R_{i-1}, R_i)$, located between radii R_{i-1} and R_i on the sky. To express his equations in terms of quantities relevant for X-ray analysis we simply associate $\mathcal{N}(R_{i-1}, R_i)$ with the X-ray flux, $F_{\text{x}}(R_{i-1}, R_i)$, in $\text{erg cm}^{-2} \text{ s}^{-1}$.

We have developed our own code to implement the deprojection algorithm and have verified it using synthetic XMM data obtained by using the QUICKSIM software (Snowden, 1999). Some aspects of the deprojection analysis require special mention which we now address.

3.1. Edge Effect

The deprojection algorithm assumes there is no source emission outside of the bounding annulus, R_m . This is generally not the case, and if the exterior emission is not accounted for then the volume emission density of the outermost annuli will be overestimated. Nulsen & Böhringer (1995) provide an analytic correction factor for the flux of the bounding annulus in the limit of annuli with zero width. Since, however, the width of the bounding annulus tends to be large because of decreasing S/N with increasing radius, and since any exterior emission also projects into interior annuli, we follow McLaughlin (1999) and compute a separate correction factor, $f(R_{i-1}, R_i)$, for each annulus arising from emission exterior to R_m .

The emissivity of this exterior emission projected into an annulus (R_{i-1}, R_i) is taken to be proportional to

$f(R_{i-1}, R_i)F_{\text{x}}(R_{m-1}, R_m)$; i.e. the spectral shape of the emission exterior to R_m is assumed to be the same as that for the outermost annulus. Moreover, to compute $f(R_{i-1}, R_i)$ a model for the spatial profile for the exterior emission is required. We assume that the volume X-ray emission density is a power law outside of R_m which is a good approximation for galaxies and groups since the X-ray emission at large radii is generally well described by a β model ($r^{-6\beta}$) with $\beta \approx 0.5$ -0.7 (e.g., Mulchaey & Zabludoff 1998). Our results are not very sensitive to these assumptions because our chosen bounding annuli are quite wide so that $f \ll 1$ for β over this range.

The formulae for $f(R_{i-1}, R_i)$ for the cases $\beta = 1/2$ and $\beta = 2/3$ are given by equations A7 and A8 in McLaughlin (1999). All results presented in §4 are for the case $\beta = 2/3$ since, as mentioned above, the results are quite insensitive to this choice. Both the numerator and denominator of McLaughlin's equation A8 evaluate to zero for $R_{i-1} = 0$ which is problematical for numerical computations. Fortunately, the limit is well-behaved, and in Appendix A we give the limiting equation.

3.2. Error Estimation

The deprojected X-ray emission in any annulus interior to the bounding annulus depends on the previous results obtained for adjacent exterior annuli. Since the deprojection procedure introduces correlations between annuli it is natural to employ Monte Carlo simulations to estimate the statistical uncertainties on the spectral parameters. Hence, after we have obtained best-fitting models for all desired annuli on the sky, we simulate a new data set for each annulus by using these models as templates. Then we deproject these simulated data and obtain parameters in the same manner as done for the actual data.

For each observation we determine the errors on each parameter from 100 Monte Carlo simulations. In most cases we found that the simulated parameters are reasonably symmetrically distributed about a central peak. Consequently, we define confidence limits for a parameter with respect to the median value from the 100 simulations. For example, after sorting the 100 values for a given parameter

into ascending order we define the 68% confidence limits to be given by the 16th and 84th values; the 90% limits are given by the 5th and 95th values, etc.

This scheme for defining confidence limits has its limitations. In some cases when the parameter has a large error the simulated distribution is very flat so that the median is not obviously the best reference point from which to define confidence limits. In such instances the 68% confidence limits defined as above do not always enclose the best-fitting value. However, we do find that in all cases the best-fitting values are enclosed with the $\sim 90\%$ confidence limits indicating that our definitions are not very unreasonable, and thus we apply the above definitions of confidence levels in every case for consistency and convenience.

3.3. Radial Parameter Fluctuations

It is well known from optical studies that the deprojection of the luminosity distribution of an elliptical galaxy yields a jagged profile where the departures from a smooth profile are of the same magnitude or larger than the statistical errors on the photometry (e.g., Binney, Davies, & Illingworth 1990). A variety of factors contribute to the high-frequency noise responsible for the jagged profile such as the incomplete removal of point sources. An analogous situation occurs for the deprojection of X-ray data.

In actuality the situation is worse for the X-ray case because one desires the profiles of several spectral parameters in addition to the luminosity, but the statistical noise is much greater while the ability to remove contaminating sources is usually much worse than in the optical. As a result, the radial fluctuations in parameter values can sometimes be sufficiently large so that the values get sent off to obscure regions of parameter space never to return. Such fluctuations do not agree with the parameters obtained from fitting the X-ray spectra without deprojection.

Our preferred means to eliminate such fluctuations is to increase the S/N by increasing the widths of the annuli. This method is very effective and has the great advantage that no theoretical prejudice is forced onto the data (other than the desire for the 2D and 3D profiles to be qualitatively similar). Although doing this removes most of the serious parameter fluctuations in our *ROSAT* observations, in many cases there is still one annulus with divergent parameter values.

Hence, to keep any remaining fluctuations in check we smooth the derived parameter distributions in a manner related to linear regularization (e.g., Press et al 1992). The problem with linear regularization is that one restricts the point-to-point variation in the parameters with a preconceived model. For example, Finoguenov & Ponman (1999) assume the smooth profiles of the temperature and abundances to be linear functions of logarithmic radius. (The amount of smoothing applied also depends on an additional weighting factor – see Finoguenov & Ponman). However, as we show in §5.2 these choices usually lead to very biased parameter profiles.

Our method of regularizing the parameters is not standard since we do not add an extra term to the χ^2 equation because it cannot be done in the current version of XSPEC (Arnaud, 1996). Instead we perform an *ex post facto* regularization by simply restricting the available range for the temperatures and Fe abundances at a given radius accord-

ing to the desired amount of smoothing. This method is simpler to implement and, we believe, allows more transparent control over the smoothing process.

To insure that we do not over-smooth our parameter profiles we do the following: (1) We always compare the results obtained from analysis with and without deprojection and require that the two cases do not differ qualitatively. (2) We only regularize the temperatures and Fe abundances and always vary the amount of smoothing for each observation until we are satisfied that significant bias is not introduced. In most cases we found that restricting the absolute values of the radial logarithmic derivatives in the temperature and Fe abundance to be less than 1 and 1.5 respectively worked well.

3.4. χ^2 Issues

All spectral fitting was performed with the software package XSPEC (Arnaud, 1996) using the χ^2 method implemented in its standard form. The weights for the χ^2 method are computed in each PI bin assuming gaussian statistics. To insure that the weights are valid in this assumption we regrouped the PI bins for each source spectrum so that each group has at least 30 counts. The extraction of spectra is discussed in the following section.

A possible concern with the interpretation of χ^2 for goodness-of-fit is that the deprojection procedure causes the emission at inner radii to depend on that from larger radii. However, the model representing the projected emission within a given annulus is taken to be exact; i.e. statistical errors from the projected emission model are not included in the deprojection method, and therefore the statistical errors in each PI bin remain those of the 2D annulus which are gaussian. We have verified the validity of using χ^2 for measuring goodness-of-fit under the standard assumption of gaussian statistics by comparing to results obtained from 2D analysis without deprojection: in all cases investigated we find that when a large improvement in χ^2 is obtained from the deprojection analysis a qualitatively consistent large improvement is also obtained with the 2D analysis.

4. SPECTRAL ANALYSIS

4.1. Preliminaries

4.1.1. Extraction of Annular Spectra

For each system we extracted spectra in concentric circular annuli located at the X-ray centroid (computed within a $2'$ radius) such that for each annulus the width was $\geq 1'$ and the background-subtracted counts was larger than some value chosen to minimize uncertainties on the spectral parameters for each system while maintaining as many annuli as possible. Data with energies ≤ 0.2 keV were excluded to insure that the PSF was $< 1'$ FWHM. For our on-axis sources $\sim 99\%$ of the PSF at 0.2 keV is contained within $R = 1'$ (Hasinger et al, 1995).

For systems possessing more than one observation (see Table 1) we extracted the source and background spectra separately from each observation and then added them together. In all such cases the observations occurred after the October 1991 gain change so the Redistribution Matrix File (RMF), which specifies the channel probability distribution for a photon, is the same for all of them. Since, however, the detector location of the annuli are in

general slightly different for the different observations because of slight aspect differences, we averaged their respective Auxiliary Response Files (ARFs) which contain the information on the effective area as a function of energy and detector location. Any background sources that were identified by visual examination of the image were masked out before the extraction.

4.1.2. Models

Since the X-ray emission of the galaxies and groups in our sample is dominated by hot gas, we use coronal plasma models as the basic component of our spectral models. We use the MEKAL plasma code which is a modification of the original MEKA code (Mewe, Gronenschild, & van den Oord 1985; Kaastra & Mewe 1993) where the Fe L shell transitions crucial to the X-ray emission of ellipticals and groups have been re-calculated (Liedahl et al, 1995); the superior performance of the MEKAL model over the Raymond-Smith code for spectral analysis of elliptical galaxies we have previously discussed in detail in Buote (1999). Because of the limited energy resolution of the PSPC, we focus on a “single-phase” description of the X-ray emission in which a single temperature component exists at each (three-dimensional) radius. As we discuss below in §5.1 we do not expect a significant “Fe Bias” resulting from the single-phase analysis. We did investigate multiphase models of the hot gas such as a two-temperature plasma and a constant-pressure cooling flow (Johnstone et al, 1992), but interesting constraints were not obtained as explained below in §4.3; see §3.1.1 of Buote (2000a) for further description of such models.

We account for absorption by our Galaxy using the photo-electric absorption cross sections according to Balucinska-Church & McCammon (1992). Although Arabadjis & Bregman (1999) point out that the He cross section at 0.15 keV is in error by 13%, since we analyze $E > 0.2$ keV we find that our fits do not change when using the Morrison & McCammon (1983) cross sections which have the correct He value. The absorber is modeled as a uniform screen at zero redshift with solar abundances. The hydrogen column density of the absorber is generally allowed to be a free parameter to indicate any additional absorption due to, e.g., intrinsic absorbing material, calibration errors, etc. We refer to this as the standard absorber model. (In PAPER3 we discuss more complex absorption models.)

As discussed in PAPER1 and PAPER3 we also find it useful to consider absorption due to an oxygen edge which we represent by the simple parameterization, $\exp[-\tau(E/E_0)^{-3}]$ for $E \geq E_0$, where E_0 is the energy of the edge in the rest frame of the galaxy or group and τ is the optical depth; i.e. τ represents an absorbing screen located at the source redshift but placed in front of the source. Partial covering models are discussed in PAPER3.

Finally, data with energies between 0.2 and 2.2 keV were included in the analysis.

4.1.3. Meteoritic Solar Abundances

Ishimaru & Arimoto (1997) have pointed out that the accepted value for the solar Fe abundance relative to H is approximately 3.24×10^{-5} by number. This value is often called the meteoritic value since it was originally obtained for meteorites, but it also agrees with recent measurements

from the solar photosphere. This is to be contrasted with the old photospheric value of Fe/H of 4.68×10^{-5} (Anders & Grevesse, 1989) that is widely used. We have decided to use the correct “meteoritic” Fe abundance for this and subsequent papers; in XSPEC we use the abundance table of Feldman (1992). However, when comparing to previous results we shall always take care to consider the factor of 1.44 between the different Fe/H values.

Iron is the only abundance that we allow to be a free parameter. All other elemental abundances are tied to iron in their solar ratios; i.e. the values of the other abundances vary with Fe in their fixed solar ratios. In a sense we are actually fitting a metallicity, but since the Fe L-shell lines dominate all other lines in the PSPC spectrum for the ~ 1 keV plasmas of bright galaxies and groups, the fitted metallicity is almost entirely determined by Fe. Hence, we shall always quote our results as Fe abundances.

4.1.4. Scaling the Background to the Source Position

The observed background spectrum obtained from regions far away from the source in general covers a different amount of detector area, requires a different detector response, and if taken from a different observation can have a different exposure time. Within XSPEC the effect of different areas and exposure times for source and background are taken into account but not different detector responses. Background spectra taken near the edge of the PSPC field suffer from vignetting which significantly reduces the count rate with respect to the source spectra near the field center. This effect is also energy dependent, and thus the spectral shape of the background is altered as well.

To properly scale the background spectrum to the source position we perform the following simple procedure. First, as explained in §2 we fit a model to the background spectrum. Let us denote the flux of this model for an energy, E , by, $F_E(r_b, A_b, t_b)$, where r_b represents the detector position, A_b the background area on the detector, and t_b , the exposure time. The corresponding flux in a given PI channel, i , predicted by this model is then,

$$F_i(r_b, A_b, t_b) = \sum_E F_E(r_b, A_b, t_b) \text{RMF}_{Ei}(r_b) \text{ARF}_E(r_b).$$

The model, F_E , is independent of the response, and thus the expected background flux in channel, i , at the source position is simply,

$$F_i(r_s, A_s, t_s) = \sum_E \left(F_E(r_b, A_b, t_b) \frac{A_s t_s}{A_b t_b} \right) \text{RMF}_{Ei}(r_s) \text{ARF}_E(r_s), \quad (1)$$

where r_s , A_s , and t_s are respectively the position, area, and exposure time for the source.

In the general case one would prefer to use the actual background data rather than a best-guess model. To do this simply scale the real background spectrum by the factors $F_i(r_s, A_s, t_s)/F_i(r_b, A_b, t_b)$ for each PI channel. These ratios are typically very insensitive to the detailed shape of the input model spectrum.

This scaling procedure was followed for NGC 5044 and 5846. For the other systems we needed to subtract a thermal component due to the extended source emission as

discussed in §1. Since for these systems the background estimate is necessarily defined by a model we used equation (1) for the scaling.

4.2. Results

We plot in Figures 1-4 the temperature and Fe abundance profiles obtained from the deprojection analysis according to the number of annuli for which useful constraints on the parameters were obtained. This categorizes the systems essentially according to the S/N of the data. Fe abundance profiles are shown for the cases where the column density of the standard absorber was (1) fixed at the Galactic value and (2) treated as a free parameter. (The temperature profiles are very similar in each case, and thus for clarity of presentation we show only the case for fixed Galactic column density.) For both the temperature and Fe abundance profiles we also show the results obtained with and without an extra oxygen edge at 0.532 keV (rest frame). The profiles of column density and edge optical depth are given in PAPER1 for NGC 1399 and 5044 and in PAPER3 for all the systems.

The deprojected temperature profiles are all very similar to the 2D profiles obtained in many previous studies with the *ROSAT* PSPC (Forman et al 1993; Ponman & Bertram 1993; David et al 1994; Trinchieri et al 1994; Rangarajan et al 1995; Kim & Fabbiano 1995; Irwin & Sarazin 1996; Jones et al 1997; Trinchieri et al 1997; Mulchaey & Zabludoff 1998; Buote 1999). As expected, our 3D profiles display a slightly steeper rise from the central minimum to the maximum at $r \sim 50$ -100 Mpc in very good agreement with the 3D profiles obtained by Finoguenov and co-workers for several systems using both *ROSAT* and *ASCA* data (Finoguenov et al 1999; Finoguenov & Ponman 1999; Finoguenov & Jones 2000). The temperature profiles also agree very well with two-temperature models of *ASCA* data (Buote 1999, 2000a).

The models with an oxygen edge tend to have lower temperatures at small radii. This can occur because lower temperature gas produces stronger oxygen lines which are absorbed by the oxygen edge. Although in most cases both models give fits of similar quality, the edge model provides a significantly better fit for some of the systems (see PAPER1 and PAPER3).

For the four systems with the highest S/N data in our sample (NGC 507, 1399, 4472, and 5044) the Fe abundance profiles obtained from models (without an oxygen edge) where the column density is treated as a free parameter are very much larger than for all models with fixed Galactic column density. Even after accounting for the differences between meteoritic and photospheric solar abundances, the Fe abundances implied by these models greatly exceed and are very inconsistent with the Fe abundances obtained from all *ASCA* studies. They are, however, consistent with previous *ROSAT* studies where the column density was treated as a free parameter (e.g., Forman et al 1993; David et al 1994).

For these systems the models with variable column density give Fe abundances that increase rapidly with decreasing radius, but the column densities (except for NGC 507) also decrease well below the Galactic values as $r \rightarrow 0$ (PAPER1 and PAPER3). Since the column densities at large radii are consistent with the Galactic values this decrease at small radii cannot be due to errors in the background

subtraction. Rather, the sub-Galactic columns and huge Fe abundances that are inconsistent with *ASCA* signals some inadequacy in the emission model. As it turns out (see Figures 1-4) except for NGC 5044 the variable-column density models with an oxygen edge give Fe abundances (and columns) that are very consistent with the fixed-column models. This gives additional support for the edge model discussed in PAPER1 and PAPER3 (though see §5.3 of PAPER3).

In most of the other systems the variable-column-density models also tend to predict sub-Galactic columns at small radii though at much lower significance. These sub-Galactic columns are also accompanied by systematically larger Fe abundances than the fixed-Galactic case, though again the edge models usually give consistent abundances for the free- and fixed-column density cases. Hence, the Fe abundance profiles which typically agree best with previous *ASCA* analyses are those obtained from models with fixed Galactic column density (with or without an edge), though variable column models with an oxygen edge yield comparable results in most cases. Since, however, the evidence for intrinsic oxygen absorption is strong for half of these systems (PAPER1 and PAPER3) we believe the models with an intrinsic oxygen edge and a standard absorber with $N_{\text{H}} = N_{\text{H}}^{\text{Gal}}$ to be the most physical of the models investigated (i.e. crosses and dotted diamonds in middle column of Figures 1 - 4).

From inspection of Figures 1-4 it is readily apparent that most of the systems have Fe abundance profiles that decrease as a function of radius. Typically within $r \sim 10$ kpc the Fe abundance ranges from $Z_{\text{Fe}} \approx 1Z_{\odot} - (\text{several})Z_{\odot}$ and decreases to $Z_{\text{Fe}} \sim 0.5Z_{\odot}$ for $r \sim 50 - 100$ kpc. We now discuss the individual systems in groups defined by the total number of annuli with interesting constraints. When comparing our Fe abundances to previous studies we implicitly account for projection effects and the different plasma codes and solar abundances used (§4.1.3).

4.2.1. Systems with 7 Annuli

In Figure 1 we display the results for the three systems where the spectral parameters are well determined in seven annuli. These observations thus generally correspond to the highest S/N data in our sample. In each case the models with an oxygen edge exhibit significant negative Fe abundance gradient, though in NGC 1399 the key evidence occurs in the central radial bin.

NGC 507: The evidence for a Fe abundance gradient is strong as is the large value in the central bin: 95% confidence lower limits are $1.3Z_{\odot}$ and $1.1Z_{\odot}$ respectively for models with and without an oxygen edge (column density fixed at Galactic). The average Fe abundance within $r = 4'$ is $\approx 1Z_{\odot}$ in excellent agreement with the value obtained by Buote & Fabian (1998) from a two-temperature model of the *ASCA* data. Our Fe abundance profile also agrees reasonably well with the 2D profile obtained in the previous *ROSAT* study by Kim & Fabbiano (1995).

NGC 1399: The Fe abundance profile is constant for $r \gtrsim 3'$, rises slightly for $r \approx 1'-2'$, and in the center has different values depending on the model. As shown in PAPER1 and PAPER3 the edge model is strongly preferred, and thus the Fe abundance is consistent with being largest at the center; note that even though the error esti-

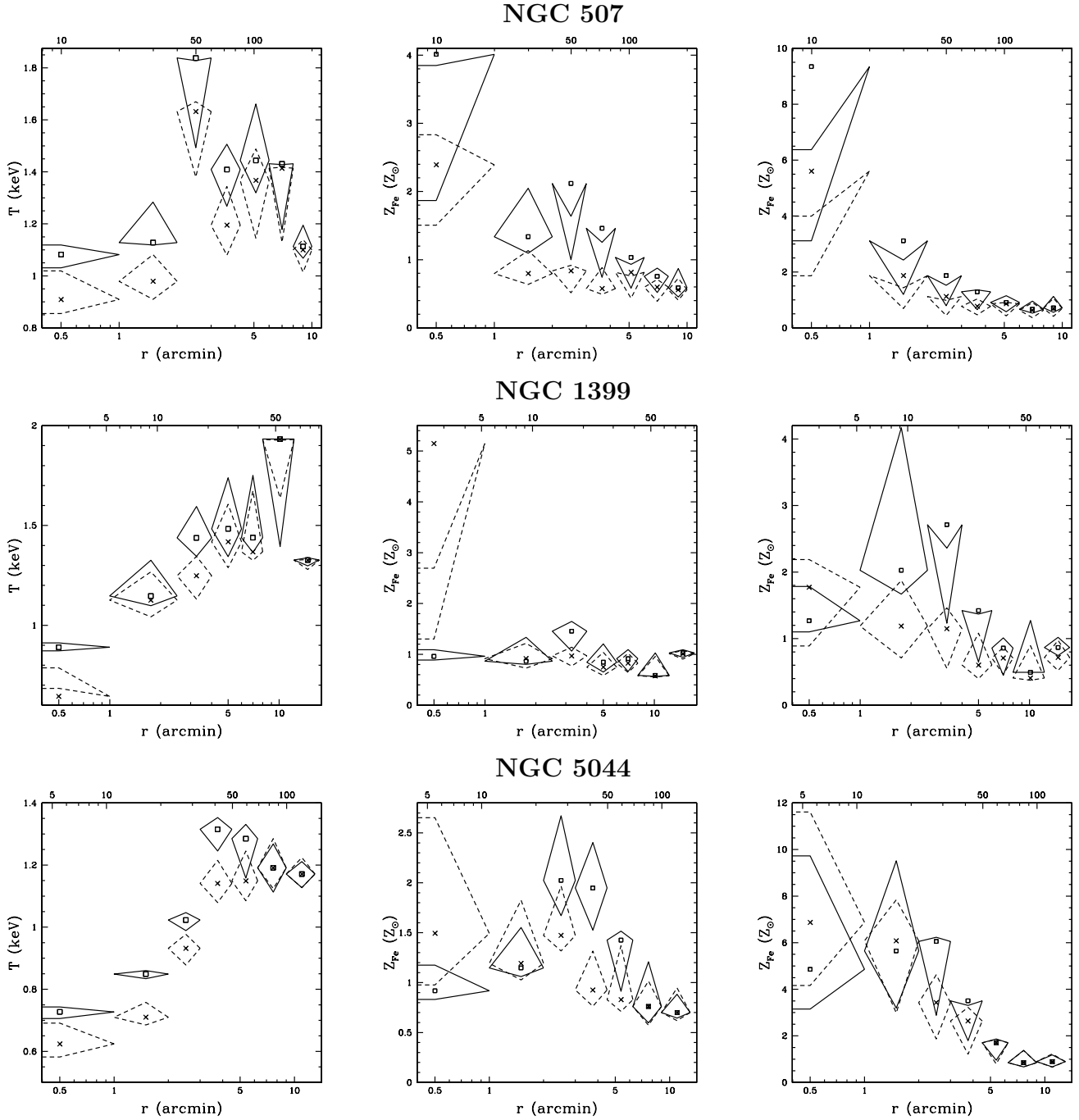


FIG. 1.— Results of the deprojection analysis for the systems where interesting constraints were obtained in 7 annuli. (Left panels) The temperature profiles for models without an oxygen edge are denoted by open squares for best fit and solid diamonds for 1σ error bars; models with an edge are represented by crosses and dashed diamonds. The column density of the standard absorber is fixed to the Galactic value in both cases. (Middle panels) The Fe abundance profiles corresponding to the temperature profiles. (Right panels) Same as the middle panels except the column density of the standard absorber is a free parameter. The radial units on the x-axis are arcminutes on the bottom and kpc on the top obtained from the redshifts assuming $H_0 = 70 \text{ km s}^{-1} \text{ Mpc}^{-1}$ and $\Omega_0 = 0.3$ except for the Virgo and Fornax systems for which a distance of 18 Mpc was assumed. See §3.2 for details on the 68% confidence error estimates.

mate for the fixed-column-density case appears to underestimate the Fe abundance, we still estimate a 95% lower limit of $1.1Z_\odot$ which is significantly greater than at large radii. The average Fe abundance within $r = 4'$ is $\approx 1.4Z_\odot$ which agrees with the lower limit obtained by Buote (1999) from a two-temperature model of the *ASCA* data and is in better agreement with a cooling flow model. Our Fe abundance profile for the case of variable column density

and no edge agrees very well with the 2D profile of Jones et al (1997).

NGC 5044: Again there is clear evidence that the Fe abundance profile is not constant with radius. As noted earlier the models with variable column density predict large Fe abundances that are inconsistent with *ASCA* studies. (But they are consistent with the previous *ROSAT* study of David et al 1994.) For example,

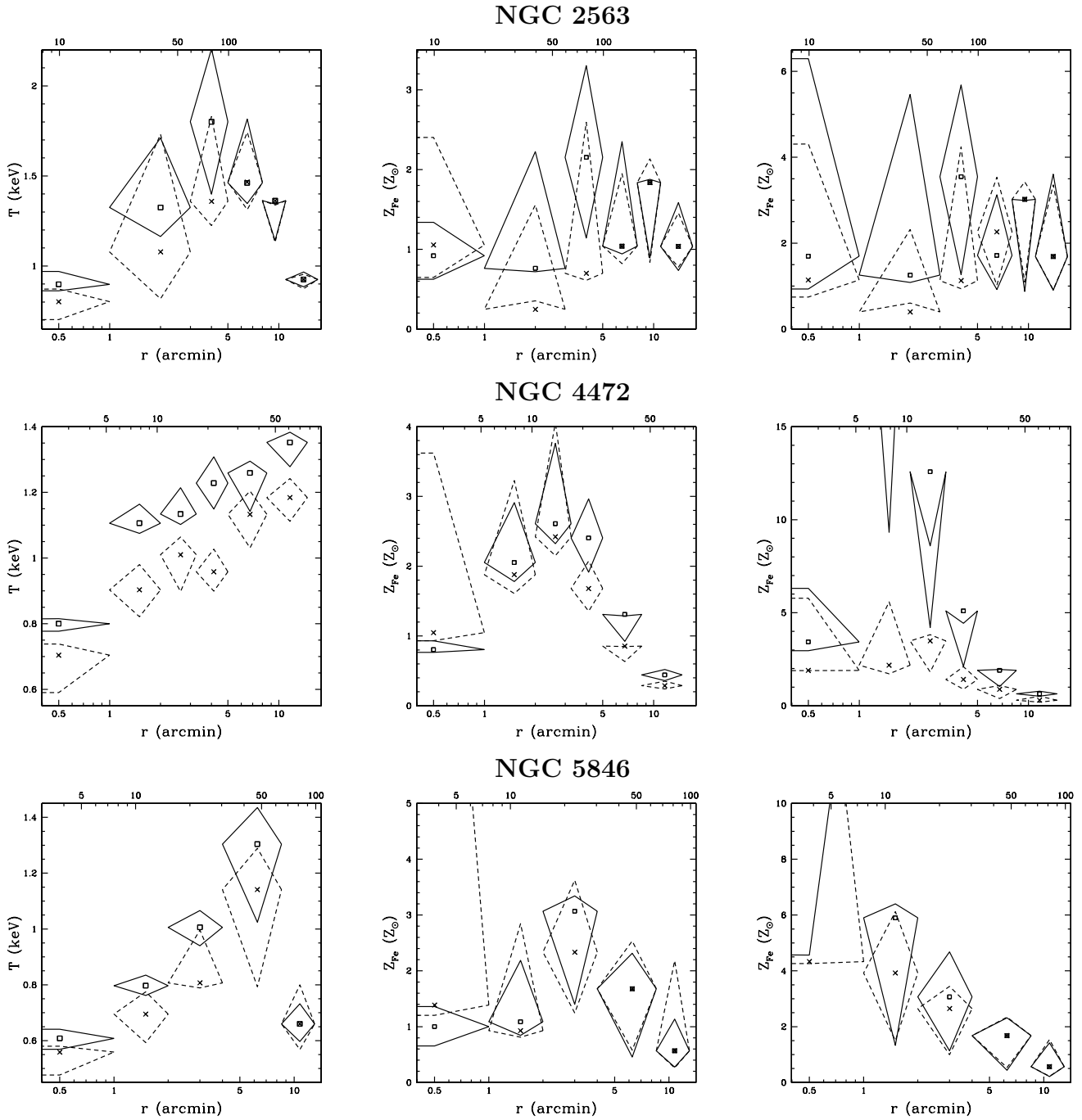


FIG. 2.— As Figure 1 but for systems with 5 or 6 annuli.

Buote (1999) obtains $Z_{\text{Fe}} \approx 0.9Z_{\odot}$ within $r \approx 5'$ for a two-temperature model of the ASCA data. Since in PAPER1 and PAPER3 we also find that an oxygen edge is clearly required in the central regions, let us focus on the Fe abundance profile obtained from a model with an edge and with fixed Galactic column density. This model yields a Fe abundance of $Z_{\text{Fe}} \sim 0.7Z_{\odot}$ for $r \gtrsim 3'$ and $Z_{\text{Fe}} \sim 1.5Z_{\odot}$ for smaller r .

4.2.2. Systems with 5-6 Annuli

The results for systems having 5 or 6 annuli are plotted in Figure 2. Evidence for a negative Fe abundance gradient is clear for NGC 4472, marginal for NGC 5846, and

non-existent for NGC 2563.

NGC 2563: Independent of the model it is clear that the Fe abundance is constant with radius with a value of $\sim 2.0Z_{\odot}$ when the column density is treated as a free parameter as opposed to $\sim 1.5Z_{\odot}$ for fixed Galactic column density. These results are consistent with the Fe abundance determined within $r \approx 3'$ by Buote (2000a) from a two-temperature model of the ASCA data.

NGC 4472: Analogously to NGC 5044 the Fe abundances obtained for the model with variable column density and no edge are very large and very inconsistent with all previous ASCA measurements. Also similar to NGC 5044 is that the edge model is strongly preferred (see PA-

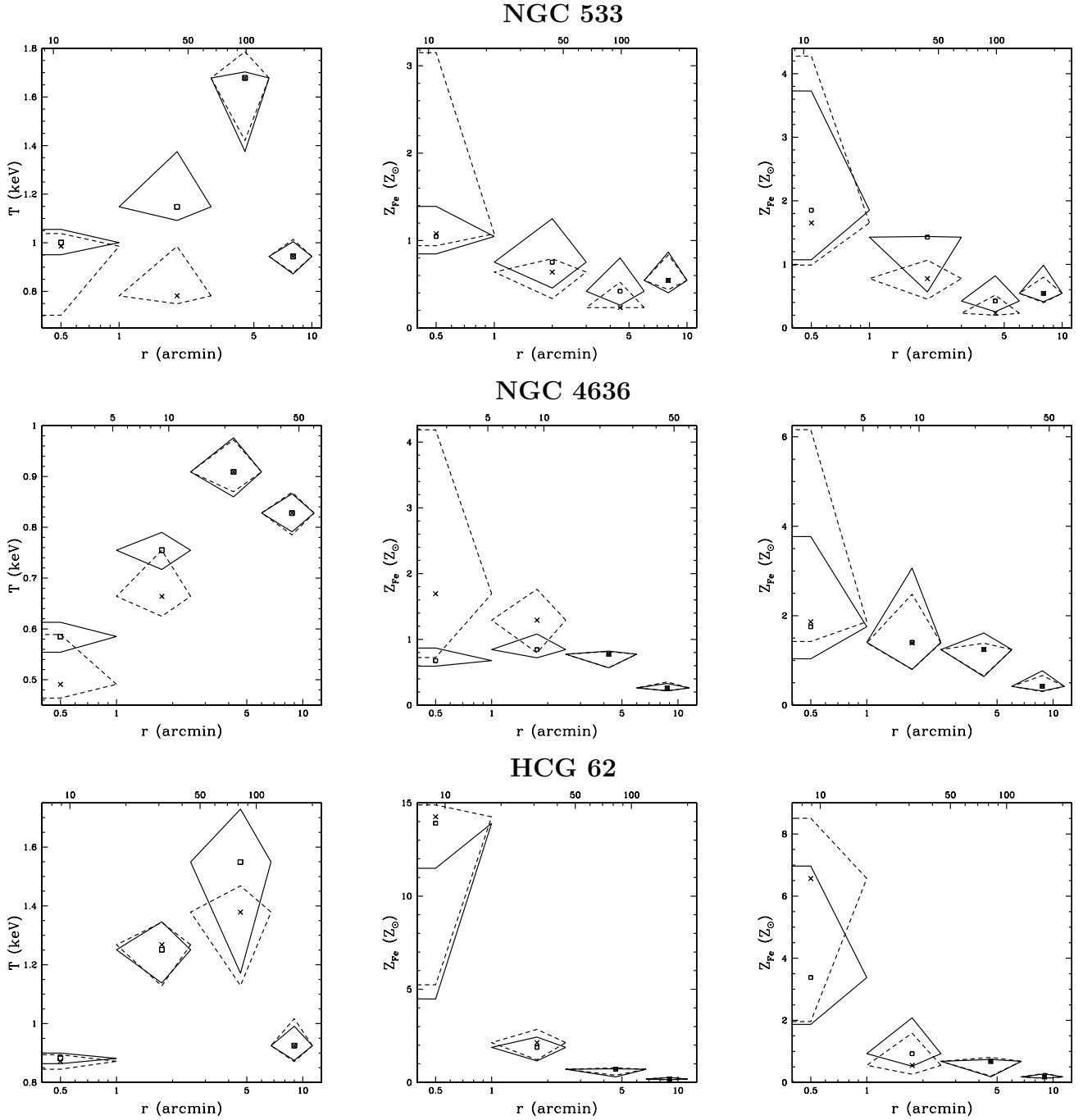


FIG. 3.— As Figure 1 but for systems with 4 annuli.

PER3). The edge models give $Z_{\text{Fe}} \lesssim 1Z_{\odot}$ for $r > 3'$ and $Z_{\text{Fe}} \sim 2Z_{\odot} - 3Z_{\odot}$ at smaller radii. These values are in excellent agreement with those obtained from previous 2D studies with *ROSAT* (Forman et al 1993; Irwin & Sarazin 1996). These Fe abundances also agree very well with the value obtained by Buote (1999) from a two-temperature model of the *ASCA* data.

NGC 5846: The models with variable column density show clear evidence for a negative Fe abundance gradient, but since the column densities obtained within the inner two bins are sub-Galactic we do not consider these models to be physical (§5.3 of PAPER3). The models with fixed Galactic column density with and without an edge give

very similar profiles except that in the central bin the upper limit on the Fe abundance for the edge model is not very well determined. These fixed-column models suggest a negative gradient in Fe abundance, but the errors are sufficiently large so that a constant profile is not clearly excluded. These Fe abundances also agree very well with the values obtained by Buote (2000a) from multitemperature models of the *ASCA* data.

4.2.3. Systems with 4 Annuli

The galaxies and groups for which we obtained useful constraints in four radial bins are shown in Figure 3. Although the data sets for these systems have lower S/N

NGC 4649

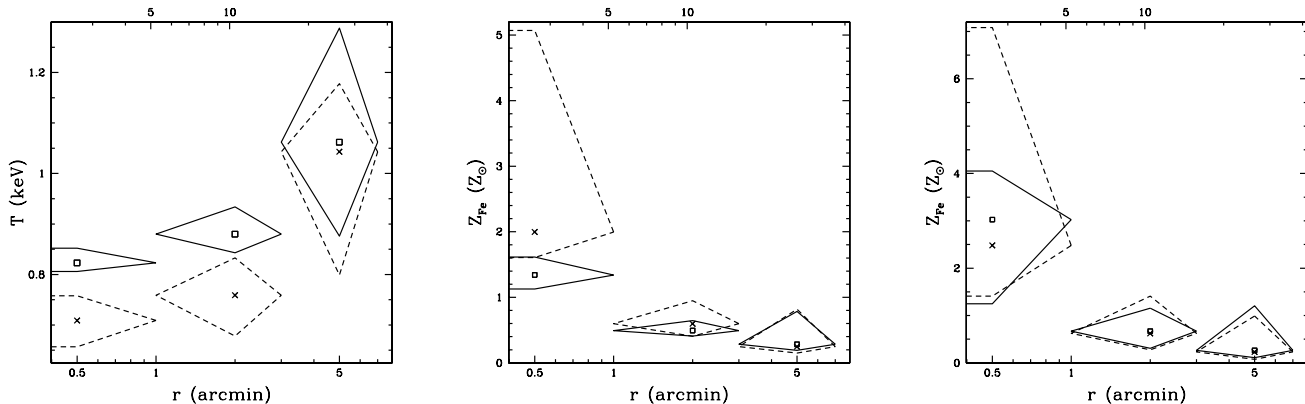


FIG. 4.— As Figure 1 but for the one system with 3 annuli.

than the previous examples, the evidence for negative Fe abundance gradients is as strong or stronger than the others.

NGC 533: All models give $Z_{\text{Fe}} \sim 0.5Z_{\odot}$ for $r \gtrsim 3'$ and $Z_{\text{Fe}} \gtrsim 1Z_{\odot}$ within $1'$. These Fe abundances are consistent with the results for multitemperature models obtained with ASCA within $r = 3'$ by Buote (2000a).

NGC 4636: In the outer bin all models give a very sub-solar value for the Fe abundance, $Z_{\text{Fe}} \sim 0.4Z_{\odot}$. The Fe abundance rises with decreasing radius such that $Z_{\text{Fe}} \gtrsim 1Z_{\odot}$ in the central bin. These results are consistent with those obtained by Buote (1999) for multitemperature models of ASCA data analyzed within $r = 5'$.

HCG 62: Similar to NGC 4636, all models give a very sub-solar value for the Fe abundance, $Z_{\text{Fe}} \sim 0.2Z_{\odot}$, in the outer bin. The Fe abundance rises very sharply with increasing radius such that $Z_{\text{Fe}} \gtrsim 2Z_{\odot}$ in the central bin. This system appears to possess the most significant Fe abundance gradient in our sample: the 95% lower limits on the values in the central bin are $4.6Z_{\odot}$ and $3.2Z_{\odot}$ respectively for models with and without an edge (both with column density fixed to Galactic). The Fe abundance of $\sim 1.4Z_{\odot}$ obtained by Buote (2000a) using a two-temperature model of the ASCA data accumulated within $r = 3'$ is consistent with our ROSAT results provided the Fe abundance in the central bin is near the estimated 1σ lower limits.

4.2.4. Systems with 3 Annuli

Finally, in Figure 4 we show the results for the galaxy with the smallest number of annuli, NGC 4649. Similar to the 4-annuli objects, NGC 4649 is one of the most significant examples for a decrease in Fe abundance with increasing radius.

NGC 4649: For this system the edge model is clearly preferred (see PAPER3), though the Fe abundances are fairly similar for all of the models. In the outer bin $Z_{\text{Fe}} \sim 0.25Z_{\odot}$ for all models and rises to $Z_{\text{Fe}} \gtrsim 1.5$ within the central bin for the edge models. Buote & Fabian (1998) obtained a Fe abundance of $\sim 1.3Z_{\odot}$ from a two-temperature model of the ASCA data within $r = 3'$ in good agreement with our ROSAT results.

4.3. Caveats

(i) *Spherical Symmetry:* The X-ray isophotes of most of the systems are approximately circular over the regions examined. Notable exceptions are NGC 1399 and 4472 which show significant deviations from circular symmetry at large radius. For $R \gtrsim 5'$ there is a significant N-S asymmetry in the X-ray surface brightness of NGC 1399 which Jones et al (1997) hypothesize is due to incomplete relaxation of the gas in the surrounding group. In contrast, outside of $R \gtrsim 3'$ the X-ray isophotes of NGC 4472 flatten which Irwin & Sarazin (1996) attribute to ram pressure as the galaxy moves with respect to the Virgo cluster. Our results for these systems at large radii average over these asymmetries. It is worth remarking that although these systems have larger than solar Fe abundances at their centers, we find that at the largest radii $Z_{\text{Fe}} \sim 0.75Z_{\odot}$ for NGC 1399 and $Z_{\text{Fe}} \sim 0.3Z_{\odot}$ for NGC 4472; i.e. it is plausible that the small value for NGC 4472 is significantly influenced by the ambient gas of the Virgo cluster.

(ii) *Single-Phase Gas:* We have focused on single-phase analysis of the hot gas because in no case did we find that multiphase models of the hot gas improved the fits significantly. In the central bins of most of the systems we expect gas to be emitting over a range of temperatures because of the observed temperature gradients. However, deprojection has removed the high-temperature gas components from the centers leaving a much smaller temperature range (typically a few tenths of a keV) which cannot be distinguished by the limited energy resolution of the PSPC. (Note that even if gas is dropping out of a cooling flow, emission weighted temperatures are within 50% of the ambient value – e.g., Buote, Canizares, & Fabian 1999). These small temperature ranges also indicate that the “Fe Bias” should be unimportant (see appendix of Buote 2000a), and thus multitemperature models do not give qualitatively different Fe abundances in the central bins – see also §5.1.

(iii) *Background Issues:* There are two backgrounds which must be considered. First, the edge effect described in §3.1 requires one to assume a model for the emission outside of the bounding annulus. We never found any noticeable effect on the derived temperatures and abundances for reasonable choices of β . Only the electron density is affected and only for the outermost annuli. Second, we examined

the effects of taking background estimates from different parts of the detector and from different fields nearby to a given object. We found that in most cases when the background level was over-estimated the Fe abundances tended to be larger than when the background was under-estimated. The size of the effect depends on many factors (e.g., S/N) though again we found that for reasonable background choices only the outermost annuli are affected as would be expected. (Of course such effects will propagate to smaller radii if the regularization criteria are not applied with care – see below.)

5. DISCUSSION AND CONCLUSIONS

Deprojection analysis of the *ROSAT* PSPC data of 10 cooling flow galaxies and groups reveals clear evidence for Fe abundances that decrease with radius in all but one system (NGC 2563). Typically $Z_{\text{Fe}} \sim 0.5Z_{\odot}$ at the largest radii examined ($r \sim 50\text{--}100$ kpc) which increases to $Z_{\text{Fe}} \approx 1Z_{\odot}$ – (several) Z_{\odot} within the central radial bin ($r \lesssim 10$ kpc). In most cases the estimated uncertainties on Z_{Fe} are large within the central bin and allow for $Z_{\text{Fe}} \gg 1Z_{\odot}$ (but never $Z_{\text{Fe}} \ll 1Z_{\odot}$). Throughout this paper we have used the “meteoritic” solar abundances (Fe/H is 3.24×10^{-5} – see Ishimaru & Arimoto 1997) which leads to Fe abundances that are a factor of 1.44 larger than previous studies that used the old “photospheric” solar value for Fe (see §4.1.3).

These 3D Fe abundance profiles are generally consistent with the original 2D *ROSAT* studies (Forman et al. 1993; David et al 1994; Kim & Fabbiano 1995; Irwin & Sarazin 1996; Jones et al 1997) after accounting for projection effects and for the different plasma codes and solar abundances used (though see below in §5.1). For all 10 systems the Fe abundances (and temperatures) that we have obtained from the deprojected *ROSAT* data agree with those we have obtained previously from analysis of the *ASCA* data accumulated within $r \sim 3'\text{--}5'$ (Buote & Fabian 1998; Buote 1999, 2000a); qualitatively similar results for some of these systems also have been recently obtained with *ASCA* data by Allen, Di Matteo, & Fabian (2000).

Therefore, within $r \sim 50$ kpc of these bright galaxies and groups the *ROSAT* and *ASCA* data clearly demonstrate that the gas is non-isothermal with approximately solar Fe abundances. We now examine whether it is the assumption of isothermality or the presence of Fe abundance gradients which accounts for the very sub-solar Fe abundances inferred by most previous *ASCA* (and some *ROSAT*) studies (see Buote 2000a for a detailed review).

5.1. Fe Bias vs Fe Gradients

Previously we have discussed how fitting a single-temperature plasma model to the soft X-ray spectrum of a bright elliptical galaxy or galaxy group that actually consists of multiple temperature components can lead to a serious underestimate of the Fe abundance (Buote & Canizares 1994; Buote & Fabian 1998; Buote 1999, 2000a). In our most comprehensive treatment to date (Buote, 2000a) we provided a physical explanation of this “Fe Bias” from examination of *ASCA* data which we now summarize in Figure 5.

The accumulated *ASCA* spectra within $r \sim 3'\text{--}5'$ of the brightest elliptical galaxies and groups (including those

in our present investigation) are well represented by two-temperature (2T) models. These 2T models are also consistent with the radial temperature gradients inferred from the *ROSAT* data within the same spatial regions (Buote 1999, 2000a). Moreover, we have verified that such 2T models continue to provide a good representation of the accumulated spectra generated by the *ROSAT* temperature profiles out to the largest radii ($\sim 15'$) investigated in our present paper whether or not the temperature rises and then falls (e.g., NGC 2563 – Figure 2) or continues to rise out to the largest radii (e.g., NGC 4472 – Figure 2). This agreement is expected because a 2T model can mimic very accurately the soft X-ray spectra of cooling flows (Buote et al, 1999).

In Figure 5 we show a simulated *ASCA* SIS spectrum of a 2T model with $Z_{\text{Fe}} = 1Z_{\odot}$ with temperatures and relative emission measures typical of the bright galaxies and groups. For this discussion we consider only the energies 0.55–1.5 keV to emphasize the Fe L lines and the lower bandpass limit of the SIS. Also shown in Figure 5 is the result of fitting a single-temperature (1T) model with Z_{Fe} fixed at $1Z_{\odot}$ to the simulated 2T spectral data. It is readily apparent that the 1T model is a poor fit to the 2T spectrum as it is too peaked near 1 keV while being deficient in emission at other energies. This behavior simply reflects the ability of the 2T model to excite Fe L lines over a wider range of energies than the 1T model. In order to force the 1T model to better fit the 2T spectrum one has to reduce the size of the peak at 1 keV which means reducing the Fe abundance. Allowing Z_{Fe} to be a free parameter results in a better (but still not good) fit and with a best-fitting value of $Z_{\text{Fe}} = 0.3Z_{\odot}$ (see Figure 5.1). It is this effect that we have termed the “Fe Bias”.

This Fe Bias is dependent on the energy resolution of the detector and is more pronounced at higher resolution which is why we have focused on the *ASCA* SIS data. But if the models in Figure 5.1 are folded with the relatively low resolution of the *ROSAT* PSPC we obtain a best-fitting value of $Z_{\text{Fe}} = 0.4Z_{\odot}$ for the 1T model, very similar to that obtained above at higher resolution with the SIS. However, it must be emphasized that this underestimate with the PSPC is achieved only if the lower limit on the bandpass is restricted to energies $\gtrsim 0.6$ keV as appropriate for the SIS. If instead the lower energy limit is reduced to 0.2 keV as is appropriate for the PSPC then we obtain $Z_{\text{Fe}} \approx 0.6 - 0.7Z_{\odot}$ for the 1T model.

This smaller underestimate occurs because while reducing the Fe abundance diminishes the line emission of the 1T model to better fit the spectral maximum near 1 keV, the continuum of the 1T model must increase to compensate for the decrease in the Fe L emission at energies near $\sim 0.8, 1.2$ keV. It also compensates for the corresponding decrease in the strong O K α emission near 0.6 keV since O (like the other elements) varies with Fe in its solar ratio (see §4.1.3).

This raising of the continuum by the 1T model generally goes unnoticed when analyzing *ASCA* data for the following reason. The *ASCA* SIS and GIS bandpasses do not extend below the energy regions shown in Figure 5, but they do include energies up to ~ 10 keV. However, the emission at higher energies is usually accounted for by introducing an additional high-temperature bremsstrahlung component (BREM) to represent emission from discrete

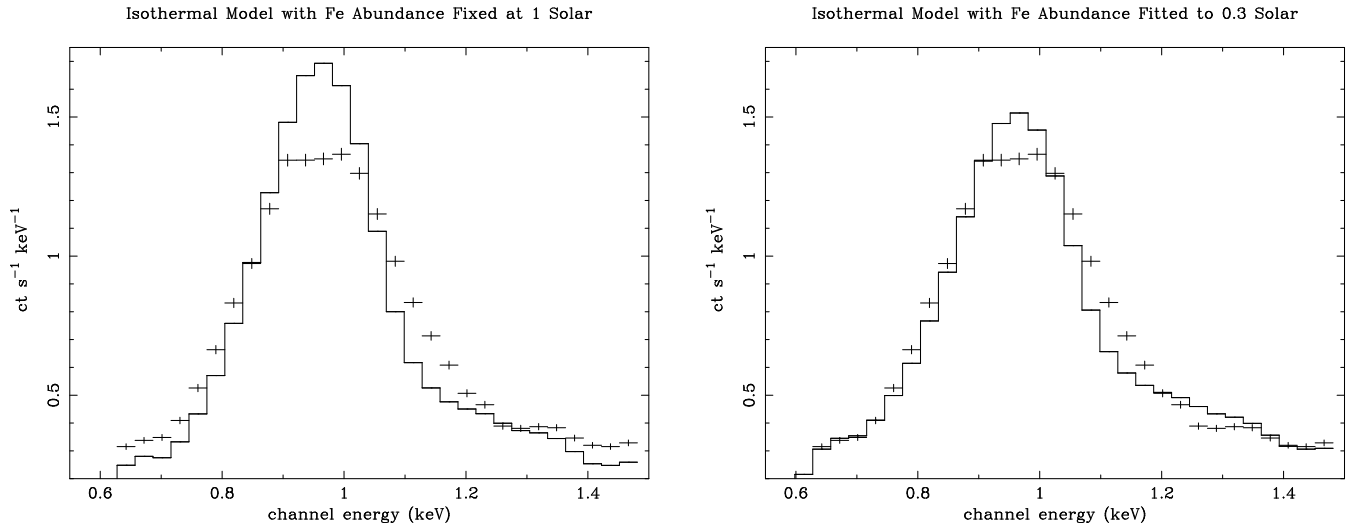


FIG. 5.— (Left) Simulated ASCA SIS spectrum of a two-temperature plasma ($T_1 = 0.75$ keV, $T_2 = 1.5$ keV with equal emission measures for each temperature component) with $Z_{\text{Fe}} = 1Z_{\odot}$ (crosses) and the best-fitting single-temperature model (solid line) also with Z_{Fe} fixed at $1Z_{\odot}$. (Right) Same but the Fe abundance of the single-temperature model is allowed to vary resulting in a best-fitting value of $Z_{\text{Fe}} = 0.3Z_{\odot}$.

sources (e.g., Matsumoto et al. 1997), and thus any increase or decrease in the emission of the 1T model at energies much larger than 1 keV can be compensated by changing the normalization of the BREM component. The required amount of compensation is generally unimportant because the emission from the 1T model decreases as $\exp(-E/T)$, and thus a plasma with $T \approx 1$ keV contributes little to the emission of a 1T+BREM model at higher energies.

However, spectral analysis with PSPC data includes lower energies (i.e. $\sim 0.2 - 0.5$ keV) that are dominated by continuum emission. The data at these energies restrict the attempt by the data near 1 keV to simultaneously reduce the Fe abundance and increase the continuum in order to force a better fit of a 1T model to the 2T spectrum. Hence, the Fe Bias affecting analysis of PSPC data is much less pronounced than for ASCA data because of the lower energy resolution of the PSPC, and especially because the PSPC data include energies below ~ 0.5 keV.

Our deprojection analysis of the PSPC data removes the temperature components projected from larger radii from the spectrum of a given annulus. Consequently, if the gas is single-phase (i.e., a single density and temperature at each radius) the range of temperatures within a given annular spectrum must be small after deprojection (i.e., essentially the temperature difference between the annuli that surround the annulus in question). Since each deprojected spectrum is nearly isothermal, and since the Fe Bias is already greatly reduced when analyzing PSPC data, we expect that the Fe Bias does not significantly affect our measurements of the Fe abundances from the PSPC data in this paper. It is therefore not surprising that the Fe abundances we have obtained from our deprojection analysis of the PSPC data agree only with those obtained from the ASCA studies that have removed the Fe bias by fitting multitemperature models of the ASCA spectra accumulated within substantial spatial regions ($r \sim 3' - 5'$; Buote & Fabian 1998; Buote 1999, 2000a; Allen et al 2000).

If a warm gas phase ($T = 10^5 - 10^6$ K) also contributes to the X-ray emission of the galaxies and groups as indi-

cated by the intrinsic absorption reported in PAPER1 and PAPER3, then the single-phase assumption needs to be reconsidered. However, the low temperature of the warm gas implies a negligible contribution to the Fe L emission and thus will not contribute to an Fe Bias. Another possibility is that the hot gas emits over a continuous range of temperatures as might be expected from an inhomogeneous cooling flow that cools at constant pressure (e.g., Johnstone et al 1992). As mentioned in §4.3 we do not find any significant change in the inferred Fe abundances if we use such a cooling flow model.

If the Fe Bias is not very important for analysis of ROSAT PSPC data, then why do some ROSAT studies find very low Fe abundances? As stated above the Fe abundances we have determined from the deprojection analysis of the PSPC data of the 10 galaxies and groups in our sample agree very well with those obtained from previous spatial-spectral analyses of these systems with the PSPC after accounting for (1) the factor of 1.44 arising from our use of the meteoritic solar abundances, (2) different plasma codes used, and (3) small differences associated with our use of a deprojection analysis (Forman et al. 1993; David et al 1994; Kim & Fabbiano 1995; Irwin & Sarazin 1996; Jones et al 1997).

Our results also agree with those of Helsdon & Ponman (2000) who fitted 1T models within large apertures (typically $20'$ radius) for several groups including NGC 533, 2563, 4636, and 5846. To make a more realistic comparison we summed up the emission models we obtained for all annuli for these systems, simulated a PSPC observation using the same exposure time, and then fitted the simulated spectrum with a 1T model like Helsdon & Ponman. The Fe abundances we obtained from this exercise are fully consistent within the 2σ errors for each system. We emphasize that Helsdon & Ponman find $Z_{\text{Fe}} \gtrsim 0.6Z_{\odot}$ (scaled to meteoritic solar) for these systems even when using very large apertures.

In contrast Mulchaey & Zabludoff (1998) obtain $Z_{\text{Fe}} \lesssim 0.2Z_{\odot}$ from 1T (Raymond-Smith) fits to the PSPC spectra of NGC 2563, HCG 62, and NGC 5846 within radii

of $\sim 20'$ (though $Z_{\text{Fe}} \sim 0.6Z_{\odot}$ is obtained for NGC 533). The values for NGC 2563 and 5846 obtained by Mulchaey & Zabludoff are inconsistent with those obtained from the very similar analysis by Helsdon & Ponman (2000) and from our deprojection analysis.

A possible explanation could be associated with the background subtraction. As we noted in §4.3 the Fe abundances will be underestimated if the background is also underestimated. This effect is only noticeable when the background is underestimated by factors of ~ 2 or more. Such a large factor will result if the background spectrum is taken from the edge of the field and not corrected for vignetting before subtracting from a source region near the center of the field. As explained in §4.1.4 we always account for the different detector responses for the source and background in our analysis.

However, when ignoring the response differences we are able to reproduce the very small Fe abundances obtained by Mulchaey & Zabludoff for NGC 2563, 5846, and HCG 62. (We perform the 1T fits in the same manner as described above for our comparison to the results of Helsdon & Ponman; i.e. we include all of the annuli investigated.) Our value for NGC 533 is consistent within the large statistical error with that obtained by Mulchaey & Zabludoff whether or not we properly scale the background to the source positions. Since the Fe abundances that we have determined from the PSPC data agree with all other previous *ROSAT* studies except Mulchaey & Zabludoff, we are lead to conclude that they must not have corrected their background spectra for vignetting before subtracting from the source spectra.

Hence, there is no evidence from the *ROSAT* PSPC data that the brightest elliptical galaxies and galaxy groups have average Fe abundances that are very sub-solar – regardless of whether they have steep Fe abundance gradients. The only clear evidence for very sub-solar Fe abundances is thus derived from fits to the *ASCA* data assuming an isothermal gas which we have shown to give misleading results because of the Fe bias. Thus, it is the assumption of isothermality, rather than the presence of Fe abundance gradients, which accounts for the very sub-solar Fe abundances inferred by most previous *ASCA* studies (see Buote 2000a for a detailed review).

5.2. Low Fe Abundance as the Result of Over-Smoothing

The consistent picture that we have described is not supported by the work of Finoguenov and co-workers who find very sub-solar Fe abundances from deprojection analysis of the *ASCA* data of HCG 62, NGC 4472, 4636, 4649, 5044, and 5846 (Finoguenov et al 1999; Finoguenov & Ponman 1999; Finoguenov & Jones 1999). For HCG 62 and NGC 5044 Finoguenov & Ponman (1999) also perform a deprojection of the *ROSAT* data and obtain results not too dissimilar from their *ASCA* analysis. As noted before in §4.2 we emphasize that our temperature profiles for these systems agree well with those obtained in the Finoguenov papers.

We have previously speculated on possible reasons for the different Fe abundances obtained by Finoguenov (see §4.1 of Buote 2000a). Now equipped with our own deprojection code we can test one of those speculations: the regularization assumptions. As discussed in §3.3 Finoguenov & Ponman (1999) require that the temperatures and abun-

dances vary approximately logarithmically with radius. However, we have shown that most of these systems, especially HCG 62, have steep Fe abundance gradients and thus these regularization criteria must be carefully checked.

In Figure 6 we plot the radial profiles of temperature and Fe abundance of HCG 62 obtained from the *ROSAT* deprojection analysis where we have used the old photospheric solar Fe abundances for consistent comparison with Finoguenov & Ponman. Because of the steep Fe abundance gradient we chose a slope of 2 to bound the radial logarithmic Fe abundance derivative. (We arrived at this choice after trying several different values and from comparison to results obtained without deprojection – see §3.3.) We also show the results when the maximum Fe abundance derivative is set to 1. These latter results agree well with the *ASCA* and *ROSAT* deprojection results of Finoguenov & Ponman; e.g., for $r \sim 30$ kpc we obtain $Z_{\text{Fe}} \sim 0.6Z_{\odot}$ which is within the 90% limits of their *ASCA* result and in excellent agreement with their *ROSAT* value. This value is to be contrasted with $Z_{\text{Fe}} \sim 1.3Z_{\odot}$ obtained at that radius when we set the maximum Fe abundance derivative to 2.

Therefore, we attribute the smaller Fe abundances obtained by Finoguenov & Ponman for HCG 62 to their overly restrictive regularization criteria. Interestingly, unlike their *ASCA* analysis of HCG 62, their *ROSAT* deprojection does not perform actual regularization but rather adopts simple smooth analytical models which apparently achieve the same effect. Finoguenov & Ponman do apply their regularization method to the deprojection of the *ROSAT* data of NGC 5044, and we can only reproduce their temperatures and small Fe abundances if we require the radial logarithmic derivatives of both the temperature and Fe abundance to be ≤ 0.2 ! In fact, given the steep Fe abundance gradients we obtain for most of the systems analyzed in the Finoguenov papers over-smoothing probably accounts for most of the Fe abundance differences between our papers.

5.3. Implications and Future Work

The Fe abundance gradients of these bright, nearby cooling flow galaxies and groups reflect the history of star formation and the dynamical evolution of the hot gas in these systems. In Figure 7 we compare the Fe abundances we have measured for NGC 4472 with those predicted from a gas-dynamical metal enrichment model which assumes (1) a Galactic IMF, (2) accretion of primordial gas arising from secondary infall, and (3) a Type Ia supernova (SNIa) rate normalized to the observed value in nearby E/S0 galaxies reported by Cappellaro et al (1997). The qualitative agreement is clear, though the deviations at larger radii indicate that the ram pressure distortions discussed by Irwin & Sarazin (1996) compromise to some extent the assumptions of spherical symmetry and hydrostatic equilibrium in the gas-dynamical model.

The relative contributions of the supernovae to the Fe abundance within ~ 50 kpc are consistent with the “solar supernova proportion” defined by Renzini et al (1993): i.e., enrichment models of the Milky Way indicate that 1/4 of the Fe in the Sun arises from Type II supernovae (SNII) and the remaining 3/4 arises from SNIa. Consequently, the approximately solar Fe abundances we have

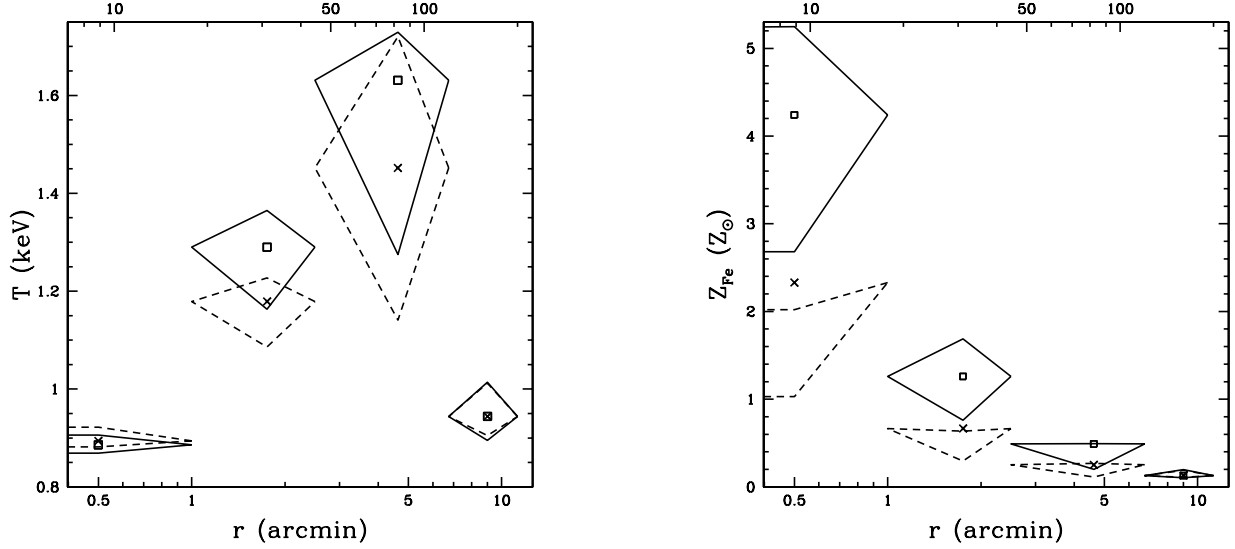


FIG. 6.— Sensitivity to regularization criteria: (Left) Temperature and (Right) Fe abundance profiles of HCG 62 obtained from deprojection analysis of the *ROSAT* data for models with fixed Galactic column density (and no added edge). The squares and solid diamonds represent models where the absolute values of the radial logarithmic derivatives of the temperature and Fe abundance are required to be ≤ 1 and ≤ 2 respectively which are the same criteria we used for the models of HCG 62 in §4.2. The crosses and dashed diamonds represent the case where the Fe abundance derivative is required to be ≤ 1 . To facilitate the comparison we have used the old photospheric solar Fe abundance (Fe/H is 4.68×10^{-5}) as is done in Finoguenov & Ponman (1999) which leads to smaller values of Z_{Fe} than obtained in Figure 3.

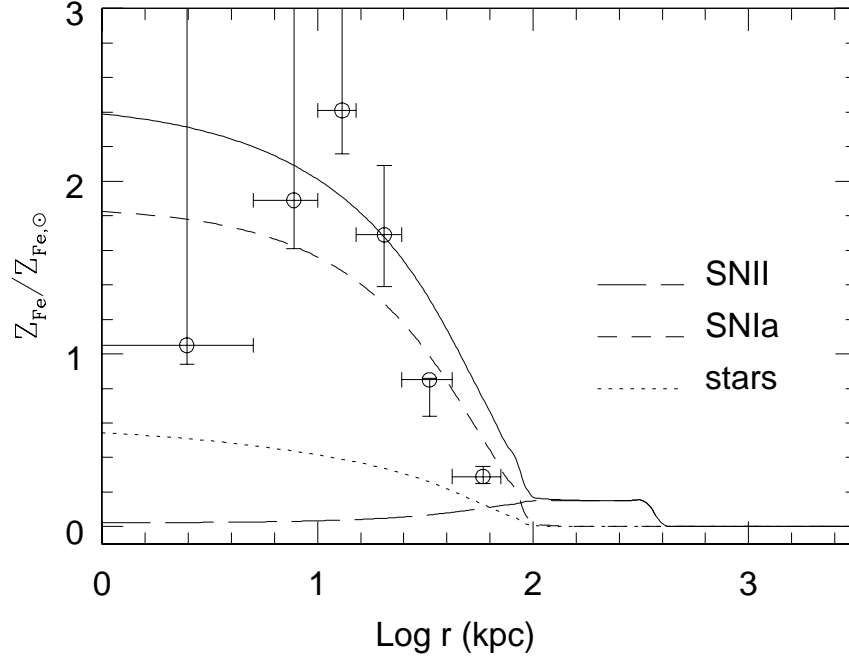


FIG. 7.— Comparison of the measured Fe abundances of NGC 4472 with a gas-dynamical metal enrichment model (F. Brighenti and W. Mathews, in preparation). The model is identical to those described by Brighenti & Mathews (1999) having a Galactic IMF and accretion of primordial gas except that the SNIa rate is normalized to the observed value in nearby E/S0 galaxies reported by Cappellaro et al (1997). The data points refer to those in Figure 2 for NGC 4472 using our favored model where the standard absorber has fixed Galactic column density and where an intrinsic oxygen edge is included in the model.

found for the brightest galaxies and groups within $r \sim 50$ kpc are consistent with models of the chemical enrichment of the Milky way and allow for the possibility of a universal IMF (e.g., Renzini et al. 1993; Renzini 1997, 2000; Wyse 1997). The problems associated with the theoretical interpretation of the very sub-solar Fe abundances inferred

from previous studies of these systems (e.g., Renzini et al. 1993; Arimoto et al. 1997; Renzini 1997) are eliminated by the approximately solar Fe abundances we have inferred from both *ASCA* and *ROSAT* data of bright galaxies and groups.

The sub-solar Fe abundances at large radii require ad-

ditional explanation, such as the dilution arising from the accretion of primordial material included in the model in Figure 7. An alternative explanation for negative Fe abundance gradients as the consequence of the sedimentation of heavier elements (Fabian & Pringle 1977; see Qin & Wu 2000 for a recent discussion) seems less plausible since the drift velocities are generally similar to or less than the flow velocities in a cooling flow.

We mention that the Fe abundance at large radius ($\gtrsim 100$ kpc) predicted by the model for NGC 4472 (Figure 7) arises entirely from SNII ejecta. These SNII explosions accompanied the initial burst of star formation which ended at a redshift before ~ 2 . Hence, the Fe abundance measured at such large radii is a direct fossil record of the ISM abundance at high redshift. For those systems where we have measured Fe abundances at $r \gtrsim 100$ kpc we find $Z_{\text{Fe}} \sim 0.5 Z_{\odot}$. If they are indeed the result of the initial SNII enrichment these large Fe abundances are consistent with the arguments that large quantities of the metals at high redshift reside in hot gaseous halos (Pettini 1999, 2000) and that there was a prompt initial enrichment of the early universe (Renzini 1997, 2000).

Finally, *Chandra* and *XMM* will substantially clarify our understanding of the metal enrichment and gas dynamics in cooling flows. Their superior spatial and spectral resolution will enable abundances to be measured on scales

$r \lesssim 1$ kpc which is critical since the *ROSAT* data suggest that the gradients may be largest at small radii (§4.2). These new missions will also allow accurate mapping of the abundances of several α elements (e.g., Si) which is of special importance because the α/Fe ratios provide the strongest constraints on the relative numbers of Type II and Type Ia supernovae. The detailed constraints on the supernovae feedback in these nearby cooling flows will be invaluable for interpreting the star formation process in galaxies at high redshift (Cavaliere et al, 2000).

It is a pleasure to thank the referee, J. Irwin, for helpful comments, F. Kelly for programming advice, and W. Mathews for permission to include Figure 7 in this paper. This research has made use of (1) data obtained through the High Energy Astrophysics Science Archive Research Center Online Service, provided by the NASA/Goddard Space Flight Center, and (2) the NASA/IPAC Extragalactic Database (NED) which is operated by the Jet Propulsion Laboratory, California Institute of Technology, under contract with NASA. Support for this work was provided by NASA through Chandra Fellowship grant PF8-10001 awarded by the Chandra Science Center, which is operated by the Smithsonian Astrophysical Observatory for NASA under contract NAS8-39073.

APPENDIX

LIMITING CASE FOR EDGE CORRECTION FACTOR

The edge correction factor, $f(R_{i-1}, R_i)$, given by equation A8 of McLaughlin (1999) evaluates to zero in both the numerator and denominator when $R_{i-1} = 0$. However, the limit is well-behaved there, and after applying L'Hôpital's rule we obtain,

$$\lim_{\epsilon \rightarrow 0} f(\epsilon, R_i) = \frac{(R_{m-1} + R_m) R_{m-1} R_m}{R_i^3} \left(-1 + \frac{2}{\pi} \left[\frac{2R_i}{R_m} + \cos^{-1} \left(\frac{R_i}{R_m} \right) - \frac{R_i}{R_m} \sqrt{1 - \frac{R_i^2}{R_m^2}} \right] \right), \quad (\text{A1})$$

where R_i is the radius of the circle in question and (R_{m-1}, R_m) are the inner and outer radii of the bounding annulus.

REFERENCES

- Allen, S. W., Di Matteo, T., & Fabian, A. C., 2000, MNRAS, in press (astro-ph/9910188)
- Anders E., & Grevesse N., 1989, *Geochimica et Cosmochimica Acta*, 53, 197
- Arabadjis, J. S., & Bregman, J. N., 1999, ApJ, 514, 607
- Arimoto, N., Matsushita, K., Ishimaru, Y., Ohashi, T., Renzini, A., 1997, ApJ, 477, 128
- Arnaud, K. A., 1988, in *Cooling Flows in Clusters of Galaxies*, ed. A. C. Fabian, (Kluwer: Dordrecht), 31
- Arnaud K., 1996, in Jacoby G. and Barnes J., eds., *Astronomical Data Analysis Software and Systems V*, ASP Conf. Series volume 101, p17
- Balucinska-Church, M., & McCammon, D., 1992, ApJ, 400, 699
- Binney, J. J., Davies, R. L., & Illingworth, G. D., 1990, ApJ, 361, 78
- Brighenti, F., & Mathews, W. G., 1999, ApJ, 515, 542
- Buote, D. A., 1999, MNRAS, 309, 695
- Buote, D. A., 2000a, MNRAS, 311, 176
- Buote, D. A., 2000b, ApJ, 532, L113(PAPER1)
- Buote, D. A., 2000c, ApJ, submitted (PAPER3) (astro-ph/0001330)
- Buote, D. A., & Canizares, C. R., 1994, ApJ, 427, 86
- Buote, D. A., & Fabian, A. C. 1998, MNRAS, 296, 977
- Buote, D. A., Canizares, C. R., & Fabian, A. C. 1999, MNRAS, 310, 483
- Cappellaro E., Turatto M., Tsvetkov D. Yu., Bartunov O. S., Pollas C., Evans R., & Hamuy M., 1997, A&A, 322, 431
- Cavaliere, A., Giacconi, R., & Menci, N., 2000, ApJLetters, in press (astro-ph/9912374)
- Chen, L.-W., Fabian, A. C., & Gendreau, K. C., 1997, MNRAS, 285, 449
- Ciotti L., D'Ercole A., Pellegrini S., & Renzini A., 1991, ApJ, 376, 380
- David L. P., Jones C., & Forman W., 1991, ApJ, 380, 39
- David, L. P., Jones, C., Forman, W., Daines, S., 1994, ApJ, 428, 544
- Dickey J. M., Lockman F. J., 1990, ARA&A, 28, 215
- Fabian A. C., 1994, ARA&A, 32, 277
- Fabian, A. C., & Pringle, J. E., 1977, MNRAS, 181, 5p
- Fabian, A. C., Hu, E. M., Cowie, L. L., Grindlay, J., 1981, ApJ, 248, 47
- Feldman U., 1992, *Physica Scripta*, 46, 202
- Finoguenov, A., & Jones, C., 1999, ApJ, submitted
- Finoguenov, A., & Ponman, T. J., 1999, MNRAS, 305, 325
- Finoguenov A., Jones C., Forman W., & David L., 1999, ApJ, 514, 844
- Forman W., Jones C., David L., Franx M., Makishima K., & Ohashi T., 1993, ApJ, 418, L55
- Hasinger, G., Boese, G., Predehl, P., Turner, T. J., Yusaf, R., George, I. M., & Rohrbach, G., 1995 MPE/OGIP Calibration Memo CAL/ROS/93-015 ver. 1995 May 8
- Helsdon, S. F., & Ponman, T. J., 2000, MNRAS, in press (astro-ph/0002051)
- Irwin, J. A., Sarazin, C. L., 1996, ApJ, 471, 663
- Ishimaru, Y., & Arimoto, N., 1997, PASJ, 49, 1
- Johnstone R. M., Fabian A. C., Edge A. C., & Thomas P. A., 1992, MNRAS, 255, 431

- Jones, C., Stern, C., Forman, W., Breen, J., David, L., Tucker, W., & Franx, M., 1997, *ApJ*, 482, 143
- Kaastra J. S., & Mewe R., 1993, *A&AS*, 97, 443
- Kim, D.-W., & Fabbiano, G., 1995, *ApJ*, 441, 182
- Kriss, G. A., Cioffi, D. F., & Canizares, C. R., 1983, *ApJ*, 272, 439
- Liedahl D. A., Osterheld A. L., & Goldstein W. H., 1995, *ApJ*, 438, L115
- Loewenstein M., Mathews W. G., 1991, *ApJ*, 373, 445
- Matsumoto H., Koyama K., Awaki H., Tsuru T., Loewenstein M., & Matsushita K., 1997, *ApJ*, 482, 133
- McLaughlin, D. E., 1999, *AJ*, 117, 2398
- Mewe R., Gronenschild E. H. B. M., & van den Oord G. H. J., 1985, *A&AS*, 62, 197
- Morrison, R., & McCammon, D., 1983, *ApJ*, 270, 119
- Mulchaey J. S., & Zabludoff A. I., 1998, *ApJ*, 496, 73
- Nulsen, P. E. J., & Böhringer, H., 1995, *MNRAS*, 274, 1093
- Pettini, M., 1999, in *Chemical Evolution from Zero to High Redshift*, ed. J. Walsh and M. Rosa (Berlin: Springer)(astro-ph/9902173)
- Pettini, M., 2000, *Philosophical Transactions of The Royal Society: Series A* (astro-ph/0001075)
- Plucinsky, P. P., Snowden, S. L., Briel, U. G., Hasinger, G., & Pfeffermann, E., 1993, *ApJ*, 418, 519
- Ponman, T. J., & Bertram, D., 1993, *Nature*, 363, 51
- Press, W. H., Teukolsky, S. A., Vetterling, W. T., & Flannery, B. P., 1992, *Numerical Recipes in C Second Edition* (Cambridge Univ. Press: Cambridge)
- Qin, B., & Wu, X.-P., 2000, *ApJ*, in press (astro-ph/9912007)
- Rangarajan, F. V. N., Fabian, A. C., Forman, W. R., & Jones, C., 1995, *MNRAS*, 272, 665
- Renzini A., Ciotti L., D’Ercole A., & Pellegrini S., 1993, *ApJ*, 419, 52
- Renzini, A., 1997, *ApJ*, 488, 35
- Renzini, A., 2000, in *Large Scale Structure in the X-Ray Universe*, ed. I. Georgantopoulos and M. Plionis (Gyf sur Yvette, Ed. Frontieres) (astro-ph/0001312)
- Sarazin, C. L., 1986, *Rev. Mod. Phys.*, 58, 1
- Snowden, S., 1999, <http://heasarc.gsfc.nasa.gov/docs/xmm/quicksim/>
- Snowden, S. L., McCammon, D., Burrows, D. N., & Mendenhall, J. A., 1994, *ApJ*, 424, 714
- Trinchieri G., Fabbiano G., Kim D.-W., 1997, *A&A*, 318, 361
- Trinchieri G., Kim D.-W., Fabbiano G., & Canizares C., 1994, *ApJ*, 428, 555
- Wyse, R. F. G., 1997, *ApJ*, 490, L69